

Reliable Motion Estimation in Super-Resolution US by Reducing the Interference of Microbubble Movement

Marion Piepenbrock, Stefanie Dencks, and Georg Schmitz

Ruhr University Bochum

Chair for Medical Engineering

Bochum, Germany

(marion.piepenbrock; stefanie.dencks; georg.schmitz)@ruhr-uni-bochum.de

Abstract—In ultrasound localization microscopy, microbubbles are localized and tracked in contrast enhanced ultrasound sequences to reconstruct the microvasculature. The accurate localization of MBs is essential to achieve super-resolved images, but it is strongly disturbed by tissue motion. Therefore, the MB positions have to be corrected for this tissue motion. Usually, a foreground-background separation is applied, to localize the MBs in the foreground, and to estimate the tissue motion in the background for the following correction of the MB positions. However, we recently showed that strong interferences can be introduced into motion estimation, depending on the choice of separation algorithm. Therefore, we propose to apply an optical flow approach to the non-separated B-mode images. During non-rigid motion estimation, the regions of the MBs are excluded. This leads to incomplete vector fields whose gaps are estimated afterwards.

With simulations, we show an improvement of the localization accuracy over other approaches proposed, e.g. a reduction of the displacement error of 40 μm to around 6 μm . On preclinical data, we achieved an increased correlation between the motion corrected frames. Furthermore, the reconstructed microvasculature appears clearer.

Index Terms—Localization of microbubbles, optical flow, ultrasound localization microscopy, super resolution, tissue motion estimation

I. INTRODUCTION

With ultrasound localization microscopy (ULM), super-resolved images of the microvasculature of organs and tumors can be evaluated. The technique is based on the localization and tracking of single microbubbles (MBs) in contrast-enhanced ultrasound (CEUS) sequences [1]. A correction for tissue motion is important to avoid artefacts because of false localizations [2]. There are several techniques for motion estimation available: Affine motion estimation with cross correlation [3], a two-stage motion correction based on an affine motion correction followed by a B-spline motion correction for non-rigid motion [4][2], several block matching [5][6] and optical flow algorithms [7].

This work was supported by the DFG under the Grants SCHM1171/4-1 and KI1072/11-1.

One challenge of tissue motion estimation in CEUS data is the disturbance by MBs. Widely used is a foreground-background separation to use the MB image for MB detection and the tissue image for motion estimation without disturbances of the MBs [2][3]. Recently, we have presented that the separation of the background can lead to uncertainties in the motion estimation [8]. Either, there are still MBs present, or the speckle is modified by the filtering and thus, errors in tissue motion estimation occur. The higher the MB-concentration, the higher is the influence of MBs. Therefore, we developed an approach to estimate the tissue motion on the unfiltered CEUS image by an optical flow approach. During motion estimation, the MBs and their point-spread functions (PSFs) are eliminated. The missing values in the vectorfields are estimated afterwards to get the complete vectorfields. For completion, we either use a motion model, computed by a principle component analysis (PCA), or the alternating least squares algorithm (ALS). Comparisons of the new approaches and the motion estimation on the separated background images are carried out on Field II simulations of CEUS sequences of non-rigid motion, as well as on preclinical mouse data.

II. MATERIAL AND METHODS

A. Optical Flow Approach

The non-rigid, in-plane tissue motion estimation is applied by an optical flow approach [9]. For the optical flow term, an L2-norm is used and the regularization is computed by an L1-norm to preserve the edges:

$$\min_{V_x, V_z} \iint_{\Omega_{\text{Tiss}}} \frac{\alpha}{2} \|\nabla f_{t2} \cdot V + f_{t2} - f_{t1}\|_2 + \beta (|\nabla V_x|_1 + |\nabla V_z|_1) dx dz \quad (1)$$

V_x and V_z are the estimated vectorfields, f_{t1} and f_{t2} frames at two time points, α and β are weighting factors.

The CEUS data points that are not influenced by the MBs' PSFs are defined as Ω_{Tiss} . Since the vectorfields are only computed for Ω_{Tiss} , incomplete vectorfields result. The missing

values at the MB positions are evaluated after the tissue motion estimation. For that, recurring motion in the US sequences is assumed. Dependent on the processed data, there are two different methods used to complete the vectorfields: the computation of a motion model with the principle component analysis (PCA) and the alternating least squares algorithm (ALS). The implementation was carried out with flexBox ([10]) which uses the Chambolle-Pock algorithm to solve minimization problems. The estimation of the missing values is carried out separately for lateral and axial displacements.

1) *Motion Model with Principle Component Analysis (PCA)*: Frames prior to the MB injection enable the tissue motion estimation without disturbing MBs. Hence, complete vectorfields V_{ref} are computed. A matrix with the vectorized vectorfields in the columns is generated and a principle component analysis (PCA) is evaluated to get the motion model

$$V_{\text{ref}} = UDU^T + \mu, \quad (2)$$

with U a matrix with the eigenvectors, D a diagonal matrix with eigenvalues and μ the vectorized mean vectorfield. The motion model is used to complete the vectorfield of each frame t after MB injection individually:

$$\min_d \|\tilde{U} \cdot D \cdot d - (\tilde{V}(t) - \tilde{\mu})\|_2^2. \quad (3)$$

Thereby, d is a vector to weight each component of the PCA. It minimizes the error between motion model and the known components of the vectorfield $(\tilde{U}, \tilde{\mu})$. The complete vectorfield V_{rec} is reconstructed with

$$V_{\text{rec}}(t) = U \cdot D \cdot d + \mu. \quad (4)$$

2) *Alternating Least-Squares Algorithm (ALS)*: If all frames contain MBs, only incomplete vectorfields are evaluated. To estimate the missing values, the alternating least-squares algorithm (ALS) [11] is applied which is generally used for matrix completion. It is based on the factorization $V_{\text{rec}} \approx P^T S$ of a matrix with the vectorized vectorfields in its columns. The missing values are estimated by minimizing the error between the known parts of the vectorfields \tilde{V} and the factorization:

$$\min_{P,S} \|\tilde{V} - \tilde{V}_{\text{rec}}\|_2 + \lambda(\|P\|_2^2 + \|S\|_2^2) \quad (5)$$

P and S are alternately estimated, using a least squares minimization. λ is a weighting factor.

B. Simulations

The simulations were carried out with the Field II toolbox in MATLAB [12]. The MBs were assumed to be point scatterers of a higher intensity that flow with random velocities along tracks of random directions, lengths and positions. The velocity range was chosen from 0.5 mm s^{-1} to 3 mm s^{-1} , according to the velocities in capillaries [13]. The tissue images were simulated using 20 scatterers per resolution cell to get tissue mimicking speckle pattern [14]. The intensities and the vector fields with non-rigid motion were chosen according to clinical datasets of a breast tumor [15]. 20 frames were simulated with

varying displacements. The scatterers were shifted from frame to frame. The transducer settings were chosen according to the clinical 10 MHz PLT 1005BT linear transducer of the Aplio 500 (Canon Medical Systems, Otawara, Japan), with a frame rate of 16 Hz. The pixel dimensions were $70 \mu\text{m}$ in lateral and axial direction. The displacements from frame to frame were $80 \mu\text{m}$ at maximum.

C. Preclinical Mouse Data

As preclinical data, a CEUS sequence of a subcutaneous mouse tumor, type A-431 is evaluated. It was acquired with a 40 MHz linear transducer of the Vevo 3100 (FUJIFILM Visualsonics, Toronto, ON, Canada). The frame rate was 56 Hz and 5120 frames were acquired. The sequence was separated into foreground (MB) and background (tissue), using a rank filter, to get the MBs' PSFs excluded during motion estimation. For processing, the CEUS sequence was subdivided into sub-sequences according to the breathing cycle, because the breathing leads to the largest displacements. Within each sequence, the tissue motion was estimated from frame to frame. These frame-to-frame displacements were accumulated to the displacement between the reference frame in each sequence and each frame of the sequence. Then, the displacement between one global reference frame and all local reference frames was computed. The final MB image was separated from the motion corrected sequence, and the MBs were detected by searching for local maxima after a convolution with a Gaussian kernel and a thresholding. Afterwards, the MBs were tracked with the Markov Chain Monte Carlo Data Association (MCMCDA) algorithm [16].

Apart from applying the new approaches with optical flow and PCA, or rather ALS, the optical flow was applied to separated foreground images. The separation was carried out with the singular value decomposition (SVD) [17] as well as with the median filter [16].

D. Quality Criteria

The accuracy of the estimated vectorfields from the simulations was evaluated by the absolute endpoint error AEE:

$$\text{AEE} = \frac{1}{N_{\text{MB}}} \sum_{i=1}^{N_{\text{MB}}} \sqrt{(V_x - V_{x,\text{GT}})^2 + (V_z - V_{z,\text{GT}})^2}. \quad (6)$$

It describes the absolute differences of the estimated and the ground truth vectorfields $V_{x,\text{GT}}$ and $V_{z,\text{GT}}$, averaged for each frame. Only the parts, influenced by the MB PSFs, which are important for the further processing, were considered.

For comparing the motion estimation results of the pre-clinical mouse data after applying the motion correction, the normalized cross correlation NCC was computed between the global reference frame f_{ref} and each motion corrected frame f_i :

$$\text{NCC} = \frac{(f_{\text{ref}} - \bar{f}_{\text{ref}}) * (f_i - \bar{f}_i)}{\sigma_{f_{\text{ref}}} \cdot \sigma_{f_i}}. \quad (7)$$

\bar{f}_{ref} and \bar{f}_i are the mean values of these considered frames, $\sigma_{f_{\text{ref}}}$ and σ_{f_i} their variance.

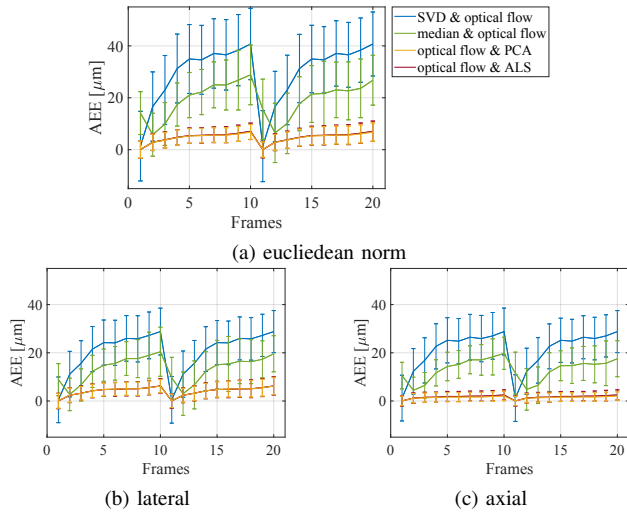


Fig. 1: Absolute endpoint error AEE of the estimated vectorfields at the MBs positions, differentiated between the Euclidean norm and the lateral and axial error. Compared are the optical flow on the separated background image after SVD (green), after median filter (blue) and the new approaches with optical flow, followed by PCA (yellow) and ALS (red).

III. RESULTS

A. Simulation Results

Fig. 1 shows the results of applying the motion estimation algorithms to the simulations. Compared are the motion estimation with optical flow on the separated background with the SVD (green) and with the median filter (blue) (method of choice in [8]) and the new approaches, the optical flow with PCA (yellow) and ALS (red). The maximum euclidean norm of the displacement error (Fig. 1(a)) is decreased from 40 μm (SVD), accordingly 25 μm with the median filter to around 6 μm with the new optical flow approaches that eliminate the MBs during motion estimation. This demonstrates the advantage of using the unprocessed data instead of calculating a background image and thus, influencing the speckle or still having the influence of MBs. The evaluation of the lateral (Fig. 1(b)) and the axial error (Fig. 1(c)) indicates that the larger error results from the lateral direction which is due to the higher resolution in axial direction. While the lateral maximum error is 6 μm with the new approach, the axial one is only 2.5 μm . In the axial direction, the error of optical flow with PCA was slightly better than the optical flow with ALS. The new approaches are both well applicable.

B. Preclinical Results

Fig. 2 and Fig. 3 show the preclinical results of the subcutaneous mouse tumor. Fig. 2 illustrates the NCC between each frame and the global reference frame. Apart from the NCC after applying the motion correction, the NCC is also computed from the original B-mode (black line). Periodically, there is a strong decorrelation (NCC of 0.74 for the B-mode data) which is due to the large displacement amplitudes during breathing. The slight decorrelations between the breathing are

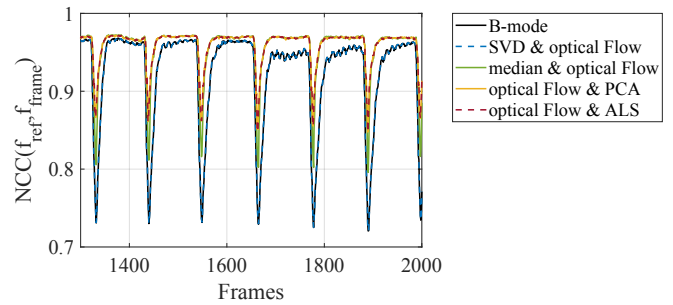


Fig. 2: Normalized cross correlation NCC between the global reference frame and each motion compensated frame. Compared are the unprocessed B-mode image (black) and the motion corrected sequences with varying methods: optical flow applied to the SVD filtered background image (blue), optical flow applied to the median filtered background image (green) and the new approaches of optical flow and PCA (yellow) and optical Flow and ALS (red).

resulting from the cardiac pulsation.

The motion estimation on the SVD filtered background (green) does not lead to significant changes in the NCC. The speckle is too strongly modified so that the tissue motion cannot be detected. The median filter before motion estimation improves the results. The minimum NCC is increased to around 0.8 which means an improvement of 5%. Additionally, the motion estimation of the frames without breathing is improved. For each motion period, the plateau is characterized by an NCC of 0.97. Hence, also the vectorfields between the different sequences (breathing periods) could successfully be computed.

The new approaches show both the same performance. Independent from using the PCA or the ALS after optical flow, the minimum NCC is increased to around 0.85 which is an improvement of 5% to the optical flow applied to the median filter and of more than 10% to the unprocessed data. The NCC in between the breathing is similar to the NCC, estimated after the median filter.

Fig. 3 shows the reconstructed microvasculature, dependent on the MB counts per pixel. The count maps after the motion estimation on the separated background images with the median filter (a) and the SVD (b) are disturbed by more artefacts than the count maps after applying the new optical flow approaches. The false detections are mainly resulting from the insufficient motion estimation during breathing. As pointed out before, the median filter leads to better results than the SVD. However, the new approaches lead to the best reconstruction, shown in (c) for the PCA and in (d) for the ALS. Hence, The new approaches enable a clearer visualization of the microvessels. By only using correlated frames that lead to a low number of false detections, less frames have to be excluded after applying the new approaches to the CEUS data than applying the optical flow to the separated background.

IV. DISCUSSION AND OUTLOOK

The new optical flow approaches improve the accuracy of MB localization in CEUS data. They strongly decrease the

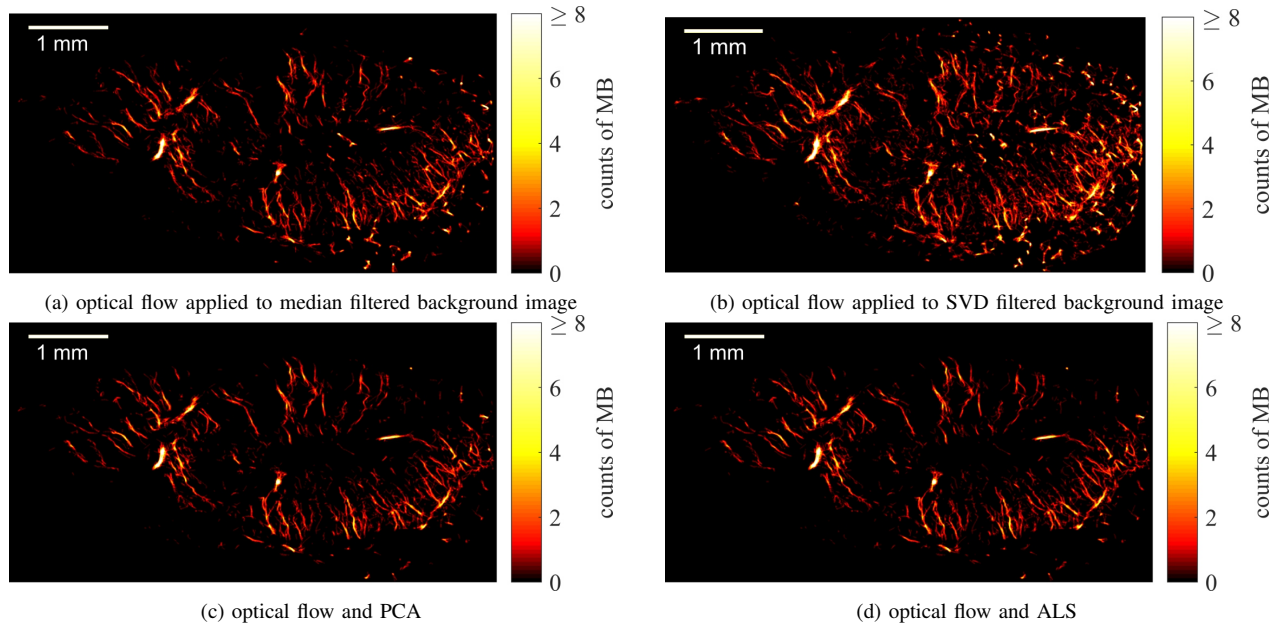


Fig. 3: Counts of MBs of a subcutaneous mouse tumor (A431) by using different techniques of tissue motion estimation (optical flow applied to background separated images and the new optical flow approaches). The MBs are localized on foreground-background separated images after motion correction, the MB tracks are estimated with the MCMCDA-Algorithm.

estimated displacement errors of tissue motion, compared to the motion estimation after foreground-background separation. The better motion estimation leads to more accurate MB localizations, but also to a lower number of false detections by applying the foreground-background separation to the motion compensated B-mode image.

The elimination of MBs during motion estimation prevents uncertainties resulting from modified speckle after filtering. This is also applicable to other types of motion estimation which shall be investigated in future work.

Especially in targets with high vascularization and strong tissue motion, as the kidney and the liver, the MBs have strong influence on the motion estimation and can thus lead to uncertainties.

ACKNOWLEDGMENT

The preclinical data were acquired by Anne Rix, Institute for Experimental Molecular Imaging, University Clinic Aachen, RWTH Aachen University, Germany.

REFERENCES

- [1] T. Opacic, S. Dencks et al., "Motion model ultrasound localization microscopy for preclinical and clinical multiparametric tumor characterization," *Nat. Comm.*, vol. 9, article number 1527, 2018.
- [2] S. Harput et al., "Two Stage Sub-Wavelength Motion Correction in Human Microvasculature for CEUS Imaging," *IEEE IUS*, 2017.
- [3] V. Hingot, C. Errico, M. Tanter, and O. Couture, "Subwavelength motion-correction for ultrafast ultrasound localization microscopy," *Ultrasonics*, vol. 77, pp. 17-21, 2017.
- [4] S. Harput et al., "Two-stage Motion Correction for Super-Resolution Ultrasound Imaging in Human Lower Limb," *IEEE TUFFC*, vol. 65, no. 5, pp. 803-814, 2018.
- [5] J. Foiret, H. Zhang, L. Mahakian, S. Tam and K. W. Ferrara, "Super-localization of contrast agents in moving organs, first experiments in a rat kidney," *IEEE IUS*, 2016.
- [6] M. McCormick, N. Rubert and T. Vaghese "Bayesian Regularization Applied to Ultrasound Strain Imaging," *IEEE Transactions on Biomedical Engineering*, vol. 58, no. 6, pp. 1612-1620, 2011.
- [7] N. Ouzir, A. Basarab, O. Lairez and J.Y. Tourneret "Robust Optical Flow Estimation in Cardiac Ultrasound Images Using a Sparse Representation," *IEEE Transactions on Medical Imaging*, vol. 38, no. 3, pp. 741-752, 2019.
- [8] M. Piepenbrock, S. Dencks, G.Schmitz, "Foreground-Background Separation Algorithms for Microbubble Localization in Ultrasound Images," *Proc. IEEE International Ultrasonics Symposium (IUS)*, pp.1-4, 2018.
- [9] B.K.P. Horn and B.G. Schunck "Determining Optical Flow," *Artificial Intelligence*, vol. 17, pp. 185-203, 1981.
- [10] H. Dirks, "A Flexible Primal-Dual Toolbox," *Cornell University Library*, arXiv:1603.05835, 2016.
- [11] B. Grung and R. Manne, "Missing values in principle component analysis," *Chemometrics and Intelligent Laboratory Systems*, no 42, pp. 125-139, 1998.
- [12] J.A. Jensen, "Field: A Program for Simulating Ultrasound Systems," *Medical & Biological Engineering & Computing*, vol. 34, pp. 351-353, 1996.
- [13] S. Stamatelos, E. Kim, A. P. Pathak, A. S. Popel, "A bioimage informatics based reconstruction of breast tumor microvasculature with computational blood flow predictions," *Microvascular research*, no 91, pp. 8-21, 2014.
- [14] T. Scabo, "Diagnostic Ultrasound Imaging: Inside Out," *Academic Press*, 2014.
- [15] S. Dencks et al, "Clinical Pilot Application of Super-resolution US Imaging in Breast Cancer," *IEEE Trans. Ultrason. Ferroelectr. Freq. Control*, 10.1109/TUFFC.2018.2872067, 2018.
- [16] D. Ackermann, G. Schmitz, "Detection and Tracking of Multiple Microbubbles in Ultrasound B-Mode Images," *IEEE TUFFC*, no 1, pp. 72-82, 2016.
- [17] C. Demené et al., "Spatiotemporal Clutter Filtering of Ultrafast Ultrasound Data Highly Increases Doppler and fUltrasound Sensitivity," *IEEE Trans. Med. Imaging*, vol. 34, no. 11, pp. 2271-2285, 2015.